PAPER

CoP for hydrogen evolution: implications from hydrogen adsorption†

Guoxiang Hu, Qing Tang and De-en Jiang*

Cobalt phosphide (CoP) is one of the most promising, earth-abundant electrocatalysts discovered to date for hydrogen evolution reaction (HER), yet the mechanism is not well understood. Since hydrogen adsorption is a key factor of HER activity, here we examine the adsorption of atomic hydrogen on the low-Miller-index surfaces of CoP, including (111), (110), (100), and (011), by using periodic density functional theory. From the calculated Gibbs free energy of adsorption, we predict that (111), (110), and (011) surfaces will have good catalytic activities for HER. From *ab initio* atomistic thermodynamics, we find that the stabilities of the surfaces at 1 atm H_2 and 300 K follow the trend of (111) > (100) ~ (110) ≫ (011). On the most stable (111) surface, both Co bridge sites and P top sites are found to be able to adsorb hydrogen with a close-to-zero free energy change and the synergy of proximal Co and P atoms on the surface results in a better HER activity. Our work provides important insights into CoP's excellent HER activity and a basis for further mechanistic understanding of HER on CoP and other transition-metal phosphides.

Introduction

Water splitting using renewable energy can provide a sustainable supply of fuel for future societies with hydrogen as a key energy carrier.[1] To date, platinum remains the most efficient electrocatalyst for hydrogen evolution reaction (HER). However, the low natural abundance and high cost of platinum hamper its wide use at the industrial scale. Thus, it is highly desirable to develop efficient, low-cost and earth-abundant electrocatalysts for HER and an enormous amount of research efforts have been devoted to it over the past decade.

Transition metal phosphides have emerged as alternative materials for HER electrocatalysts due to their high catalytic activities compared to other non-precious electrocatalysts and their relatively low costs compared to platinum. For example, phosphides of nickel,[2–13] cobalt,[14–33] iron,[34–38] copper,[39] molybdenum,[40–45] and tungsten[46] have been found to electrocatalytically generate hydrogen with low overpotentials at operationally relevant current densities. In particular, the cobalt phosphide system, which has been studied extensively, exhibits high HER activities and high stabilities under strongly acidic conditions across a diverse group of morphologies, characteristic grain sizes, support materials, and synthetic preparations. Among these systems, multi-faceted single-crystalline cobalt phosphide

(CoP) nanoparticles deposited on a titanium foil electrode exhibit outstanding activities, with overpotentials of only −70 and −85 mV (at a loading density of ~2 mg cm⁻²) to produce cathodic current densities of −10 and −20 mA cm⁻², respectively.[14] Despite the exciting experimental results of CoP, the mechanism of HER on CoP is not well understood, which is essential for further improving the activities and stabilities of the HER electrocatalysts.

Two types of possible pathways have been proposed for the mechanism of HER in acid media: the Volmer–Heyrovsky *vs.* the Volmer–Tafel mechanism. The Volmer reaction refers to the initial adsorption of protons from the acid solution to form adsorbed H ($H^+ + e^- \rightarrow H_{ad}$).[47] In the Volmer–Heyrovsky mechanism, a solvated proton from the water layer reacts with one adsorbed surface hydrogen to form H_2 ($H_{ad} + H^+ + e^- \rightarrow H_2$),[48] while in the Volmer–Tafel mechanism, two adsorbed surface hydrogens next to each other react to form an H_2 molecule ($H_{ad} + H_{ad} \rightarrow H_2$).[49] Thus, good HER electrocatalysts should be able to attract protons from the solution, while still can desorb H_2. Nørskov and coworkers have correlated experimental exchange currents with calculated hydrogen adsorption energies from density functional theory (DFT), where maximum activity is obtainable when Gibbs free energy of hydrogen adsorption (ΔG_H) is zero.[50] This is mainly because lower ΔG_H results in a very strong binding of the atomic hydrogen and hinders desorption of H_2, while higher ΔG_H prevents the binding of atomic hydrogen on the catalyst surfaces. Both of them will slow the reaction. Therefore, ΔG_H is considered as a good descriptor of HER activity, and good HER electrocatalysts are expected to have close-to-zero ΔG_H.

Department of Chemistry, University of California, Riverside, CA 92521, USA.
E-mail: de-en.jiang@ucr.edu

To understand HER on CoP in particular and to provide insights and guidelines for designing transition metal phosphide HER electrocatalysts in general, herein we have studied in detail the adsorption structures and energetics of atomic hydrogen on several low-Miller-index surfaces of CoP from first principles DFT. We use the calculated ΔG_H to predict the HER activities of the surfaces. We further employ *ab initio* atomistic thermodynamics to determine the most stable and active surface of CoP at 1 atm H_2 pressure and 300 K.

Computational

Spin-polarized DFT calculations were performed by using the Vienna *ab initio* simulation package (VASP).[51] The ion-electron interaction was described with the projector augmented wave (PAW) method.[52] Electron exchange–correlation was represented by the functional of Perdew, Burke and Ernzerhof (PBE) of generalized gradient approximation (GGA).[53] A cutoff energy of 400 eV was used for the plane-wave basis set. (111), (110), (100), and (011) surfaces were examined. About 10 Å thick slabs in (2 × 2) lateral cells with 15 Å of vacuum along the z-direction were used to model the adsorbate–surface systems for (111), (110), (100), and (011) surfaces; the Brillouin zone was sampled by (3 × 3 × 1) Monkhorst–Pack k-point mesh. Both the layer thickness and k-point mesh were tested to achieve a convergence of hydrogen adsorption energy within 0.04 eV. The top half of the slab was allowed to relax together with the adsorbed H atoms and the convergence threshold for structural optimization was set to be 0.025 eV Å^{-1} in force. Partial atomic charges were obtained using Bader charge analysis as implemented by Henkelman and co-workers.[54] We also used a different method[55] to derive the atomic charges based on the electrostatic potential, called the ESP charges.

Surface energies was determined by using

$$\gamma = \frac{E_{slab} - NE_{bulk}}{2A} \quad (1)$$

where E_{slab} is the total energy of the surface slab, E_{bulk} is the total energy of the bulk unit cell (eV per CoP), N is the number of unit formula in the slab, and A is the surface area. The differential hydrogen adsorption energy ΔE_H was calculated by

$$\Delta E_H = E(CoP + nH) - E[CoP + (n-1)H] - \frac{1}{2}E(H_2) \quad (2)$$

where $E(CoP + nH)$ and $E[CoP + (n-1)H]$ represent the total energy of the CoP system with n and $n-1$ adsorbed hydrogen atoms on the surface, respectively, and $E(H_2)$ represents the total energy of a gas phase H_2 molecule. A negative value of ΔE_H suggests favorable absorption. The differential Gibbs free energy of adsorption ΔG_H was obtained by

$$\Delta G_H = \Delta E_H + \Delta E_{ZPE} - T\Delta S_H \quad (3)$$

where ΔE_{ZPE} is the difference in zero point energy between the adsorbed H and H in the gas phase H_2 molecule, and ΔS_H is the entropy difference between the adsorbed H and H_2 in the gas phase at standard conditions. To locate the most stable

configuration for each coverage of H on a surface, we allowed the H atoms to first find the lowest energy sites and then fill the next lowest-energy sites and continue until the desired coverage was reached. In other words, we focused on finding the global minimum of hydrogen adsorption, with an assumption that the diffusion of H atoms on the surface would be facile and they always go to the lowest-energy sites.

Ab initio atomistic thermodynamics[56] was used to identify the most stable phase of each surface at 1 atm H_2 and 300 K. The Gibbs free energy of adsorption at a specific temperature and pressure $\Delta G^{ad}(T,p)$ was calculated by

$$\Delta G^{ad}(T,p) = \frac{1}{A}\left[E^{total}(N_H) - E^{total}(0) - \frac{N_H}{2}E^{total}_{H_2} - N_H\Delta\mu_H(T,p)\right]$$
$$(4)$$

where $E^{total}(N_H)$ is the total energy of the CoP system with N_H hydrogen atoms adsorbed on the surface, $E^{total}(0)$ is the total energy of the clean CoP surface, and $E^{total}_{H_2}$ is the total energy of a gas phase H_2 molecule. $\Delta\mu_H(T,p)$ is the chemical potential of hydrogen at different temperatures and pressures. Eqn (4) allows one to plot the Gibbs free energy of adsorption as a function of the hydrogen chemical potential for a specific surface at a specific H coverage. At any given hydrogen chemical potential, the stability of these H-covered surfaces can then be compared. $\Delta\mu_H(T,p)$ is related to specific (T,p)-conditions by

$$\Delta\mu_H(T,p) = \Delta\mu_H(T,p^0) + \frac{1}{2}k_B T\ln\left(\frac{p}{p^0}\right) \quad (5)$$

where $\Delta\mu_H(T,p^0)$ is the hydrogen chemical potential at the standard pressure which can be looked up from the thermodynamic tables.[57]

Results and discussion

We start with the bulk structure of CoP, followed by the clean surfaces including (111), (110), (100), and (011). We then examine and compare hydrogen adsorption on these surfaces.

Bulk CoP

Bulk CoP has a B31 or MnP-type structure, with a symmetry group of *Pnma*. In this type of structure, each metal atom is surrounded by six phosphorous atoms situated in a distorted octahedral configuration (Fig. 1a), while each phosphorous atom is surrounded by six metal atoms forming a highly distorted triangular prism (Fig. 1b). The experimental[58] and calculated lattice parameters of bulk CoP are listed in Table 1. One can see that they are in good agreement.

Clean surfaces

Low Miller-index surfaces are usually considered first in surface science studies due to their higher stabilities than higher index surfaces. We consider here four such surfaces: (111), (110), (100), and (011). Fig. 2 shows the structures of these clean CoP surfaces and Table 2 shows their calculated surface energies. One can see
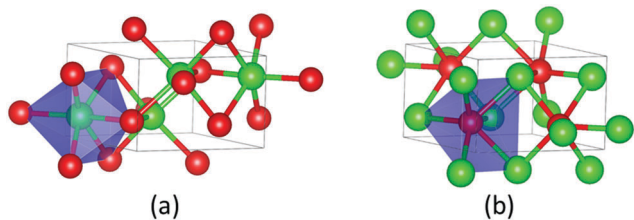
This journal is © the Owner Societies 2016

Phys. Chem. Chem. Phys., 2016, **18**, 23864–23871 | **23865**

Fig. 1 Bulk CoP: (a) each Co atom is surrounded by six P atoms situated in a distorted octahedral configuration; (b) each P atom is surrounded by six Co atoms at the corners of a highly distorted triangular prism. Co, green; P, red.

Table 1 Comparison of experimental[58] and calculated lattice parameters of the bulk CoP

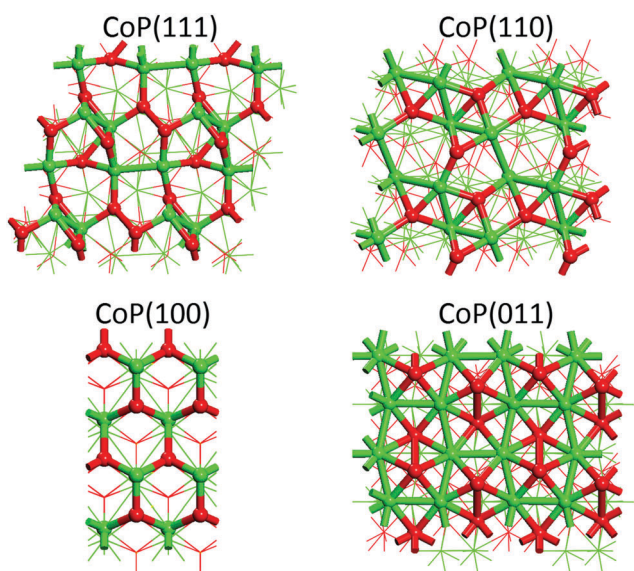| Lattice parameter	a (Å)	b (Å)	c (Å)
Experimental	5.077	3.281	5.587
Calculated	5.070	3.265	5.545

Fig. 2 Top views of clean CoP surfaces. Co, green; P, red.

that the stabilities of the clean surfaces in vacuum follow the trend of (011) > (110) > (111) > (100). In general, surfaces with higher atom packing densities are expected to have higher stabilities. Here, we find that the surface packing densities of (011), (110), (111), and (100) are 25, 24, 24, and 22 atom per nm², respectively, which indeed confirms the highest stability of the (011) surface and the lowest stability of the (100) surface. To learn the electronic structures of these surfaces, their electronic density of states (DOS) have been calculated. As shown in Fig. 3, they are all metallic and have non-zero DOS at the Fermi level. Being the

Table 2 Calculated surface energies of clean CoP surfaces

	CoP(111)	CoP(110)	CoP(100)	CoP(011)
Surface energy (meV Å⁻²)	140.4	117.0	151.0	70.4

most stable one, the (011) surface also has the lowest DOS at the Fermi level.

Hydrogen adsorption on the CoP(111) surface

As mentioned in the Introduction, ΔG_H is considered as a descriptor of HER activity, and good HER electrocatalysts should have close-to-zero ΔG_H. We next show the structures and ΔG_H of H adsorption on the four CoP surfaces. Fig. 4 shows the calculated ΔG_H and ΔE_H for CoP(111) at different hydrogen coverages (here 100% coverage = 11 H-atom per nm²). ΔG_H is more positive than ΔE_H because ΔS is negative when referencing to the H_2 state and the $T\Delta S$ term is roughly constant at −0.18 eV across the coverage range. One can see that ΔG_H is close-to-zero for 25–75% hydrogen coverage, indicating that the (111) surface will have good catalytic activity for HER at this coverage range. This supports the previous experimental finding that CoP nanostructures exposing predominately (111) surface have high HER activities.[23] The other interesting finding of H adsorption on CoP(111) is that ΔG_H shows a zigzag pattern with H coverage from 25% to 75%, which closely correlates with the adsorption sites, as discussed next.

Fig. 5 shows the optimized structures of CoP(111) with different hydrogen coverages. We find four types of stable hydrogen adsorption sites on CoP(111). For the first 25% hydrogen atoms, they are strongly adsorbed at cobalt bridge sites. During 25–75% hydrogen coverage, there is an alternative adsorption between cobalt bridge sites and phosphorous top sites, leading to a zigzagged ΔG_H with a small fluctuation. More important, ΔG_H is close-to-zero during this range, so both cobalt bridge sites and phosphorous top sites could be the active sites for HER on the (111) surface. For the 75% to 100% coverage, the extra hydrogen atoms are adsorbed at cobalt top sites, leading to more than one hydrogen atoms on some cobalt atoms.

The "zigzag" pattern between 25% and 75% hydrogen coverage suggests a synergy between proximal cobalt and phosphorous sites in adsorbing H atoms, conductive to HER. To understand this behavior, Table 3 shows differential hydrogen adsorption energies (ΔE_H) at the phosphorous top site at 0% and 31% hydrogen coverages. One can see that when there is no hydrogen adsorbed on Co (0%), the interaction of H with P is weak but when there are hydrogens already adsorbed on Co (31%), the H–P interaction becomes stronger. In other words, hydrogen adsorption at Co facilitates hydrogen adsorption at P. We found that this is due to the weakening of the Co–P bond induced by hydrogen adsorption on Co, as evidenced by the increasing Co–P bond length, which results in less negative charge on P (both Bader[54] and ESP[55] charges show the same trend) and stronger H–P covalent bonding. This synergy between Co and P for adsorbing H, as shown in Scheme 1, could be a key to CoP's high HER activity.

To evaluate the most stable coverage of H on CoP(111) at the experimental HER conditions (1 atm H_2 and 300 K), we used *ab initio* atomistic thermodynamics to determine $\Delta G^{ad}(T,p)$ as a function of hydrogen chemical potential ($\Delta\mu_H$) or pressure at T = 300 K. Fig. 6 shows the calculated $\Delta G^{ad}(T,p)$ *vs.* $\Delta\mu_H$ relationship: each line represents a given H coverage. One can
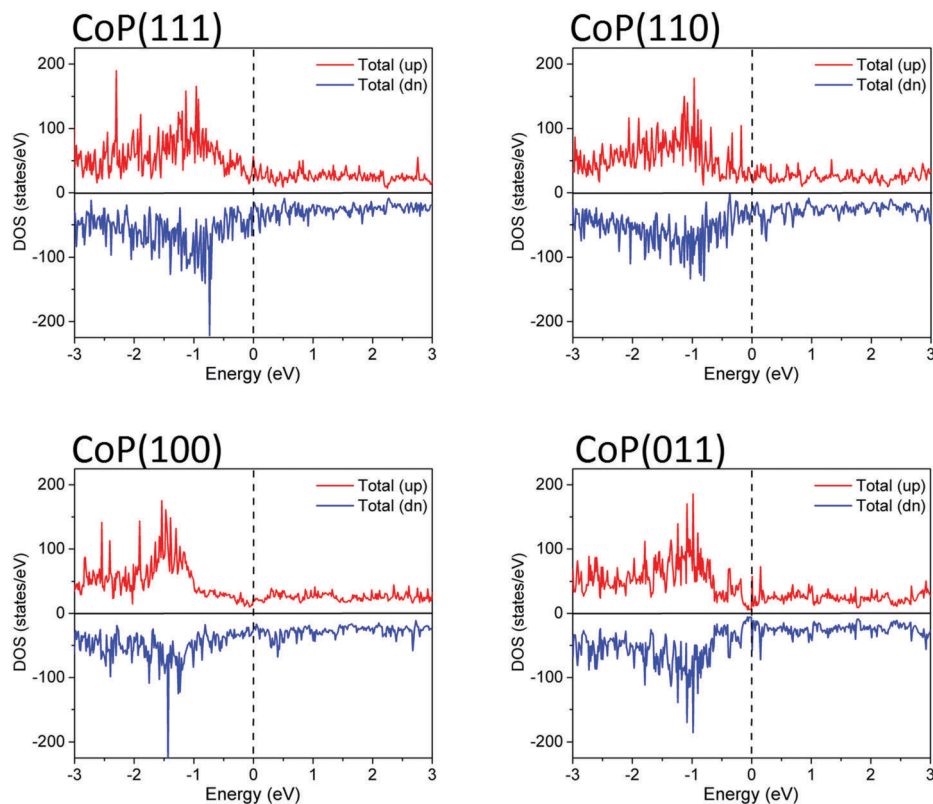
Fig. 3 Spin-polarized total electronic density of states (DOS) of clean CoP surfaces. The Fermi level (dashed line) is set as zero.
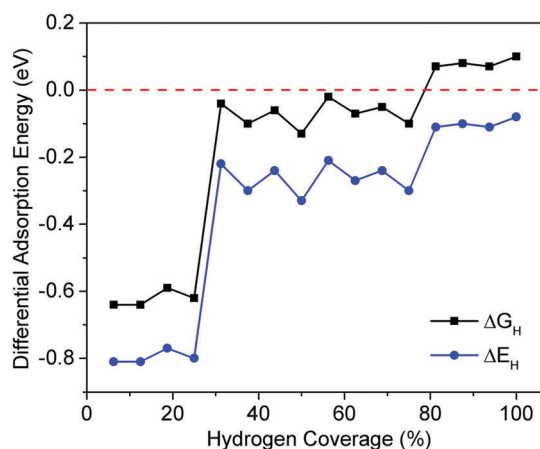

Fig. 4 Differential adsorption energy (ΔE_H) and adsorption free energy (ΔG_H) as a function of hydrogen coverage on CoP(111).
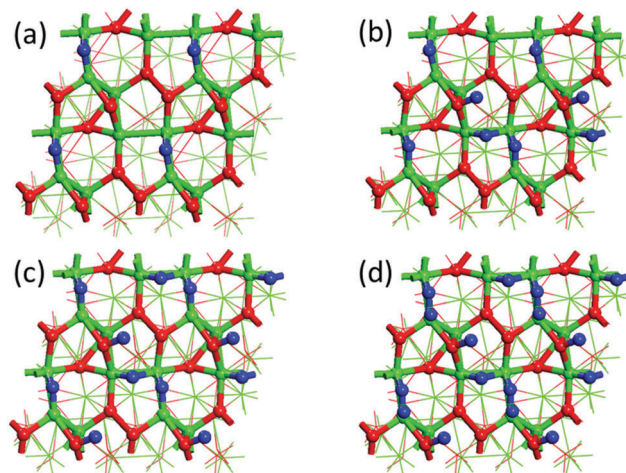

Fig. 5 Optimized structures of CoP(111) at different H coverages: (a) 25%; (b) 50%; (c) 75%; (d) 100%. 100% coverage = 11 H-atom per nm². H, blue; Co, green; P, red.

see that at extremely low hydrogen pressure, clean surface is the most stable, while at very high hydrogen pressure, 100% hydrogen coverage is the most stable (Fig. 6a). At ambient pressures, Fig. 6b shows that 75% hydrogen coverage is the most stable with ΔG^{ad} = −19.53 meV Å^{-2} at 1 atm. At this coverage, both Co and P sites adsorb H.

Hydrogen adsorption on the CoP(110) surface

Fig. 7 shows ΔG_H and ΔE_H for the CoP(110) surface at different hydrogen coverages (100% coverage = 12 H-atom per nm²).

For a favorable adsorption ($\Delta G_H < 0$), we found that ΔG_H is close to zero when hydrogen coverage is in the range of 25–50% ($\Delta G_H \sim -0.10$ eV). When hydrogen coverage is above 50%, ΔG_H is slightly positive but also close to zero. Fig. 7 suggests that the CoP(110) surface can also be good for HER activity for a large range of H coverage. Fig. S1 (ESI†) shows the optimized structures of CoP(110) at different hydrogen coverages. From 0% to 100% coverage, hydrogen atoms occupy cobalt bridge

This journal is © the Owner Societies 2016

Phys. Chem. Chem. Phys., 2016, **18**, 23864–23871 | **23867**

Table 3 Differential hydrogen adsorption energies (ΔE_H) at the P site, Co–P bond length (r_{Co-P}), and partial atomic charges on P at 0% and 31% hydrogen coverages from Bader analysis (P_{Bader}) and electrostatic potential (P_{ESP})

Hydrogen coverage	0%	31%
ΔE_H (eV)	−0.10	−0.30
r_{Co-P} (Å)	2.125	2.197
P_{Bader} ($|e|$)	−0.257	−0.213
P_{ESP} ($|e|$)	−0.308	−0.266
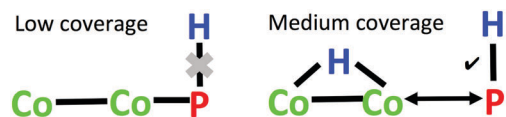
Scheme 1 The synergy between Co and P on CoP(111) in adsorbing H at medium coverage.

Fig. 7 Differential adsorption energy (ΔE_H) and adsorption free energy (ΔG_H) as a function of hydrogen coverage on CoP(110).

sites, phosphorous top sites, cobalt top sites, and another kind of cobalt top sites successively. Fig. 8 plots ΔG^{ad} as a function of $\Delta \mu_H$ for CoP(110) at different hydrogen coverages. One can see that 50% hydrogen coverage is the most stable at 1 atm and 300 K with $\Delta G^{ad} = -13.37$ meV Å^{-2}. At this coverage, Fig. 7 and Fig. S1 (in the ESI†) suggest that both the P and Co top sites are most likely to be active for HER.

Hydrogen adsorption on the CoP(100) surface

Fig. 9a shows ΔG_H and ΔE_H for CoP(100) at different hydrogen coverages. One can see that there is no H coverage where $\Delta G_H \sim 0$, so CoP(100) is not likely to be good for HER. Fig. S2 in ESI† shows the optimized structures of CoP(100) with different hydrogen coverages. We find two types of stable hydrogen adsorption sites on CoP(100): cobalt bridge sites for the first 33% hydrogen atoms and cobalt top sites for the following 67% hydrogen atoms. Unlike (111) and (110) surfaces, only cobalt atoms adsorb hydrogen on the (100) surface.
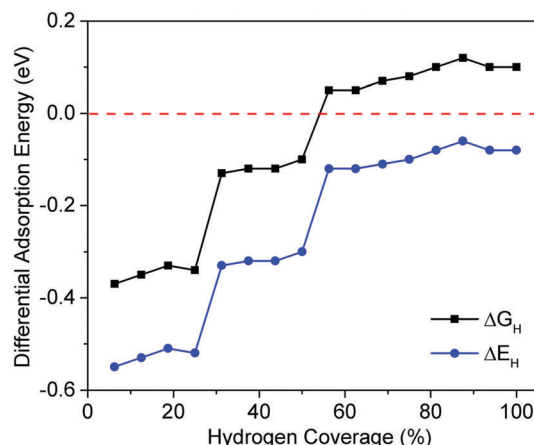
This might be the reason why we do not find $\Delta G_H \sim 0$ on CoP(100). Fig. 9b plots ΔG^{ad} as a function of $\Delta \mu_H$ for CoP(100) and we find that 33% hydrogen coverage is the most stable at 1 atm and 300 K with $\Delta G^{ad} = -13.56$ meV Å^{-2}.

Hydrogen adsorption on the CoP(011) surface

Fig. 10a shows ΔG_H and ΔE_H for CoP(011) at different hydrogen coverages. One can see that the adsorption of H on CoP(011) is in general much weaker than on the other three surfaces. On the other hand, this leads to a quite large range of H coverages from 0 to 50% where $\Delta G_H \sim 0$, indicating that CoP(011) may have good activity for HER. Fig. S3 in ESI† shows the optimized structures of CoP(011) surface at different hydrogen coverages. We find two types of stable hydrogen adsorption sites on CoP(011). The first 50% coverage of hydrogen atoms prefer phosphorous top sites with $\Delta G_H \sim 0$, so phosphorous top sites could be the active sites for HER on the (011) surface. This is in agreement with a recent study.[33] The last 50% coverage of
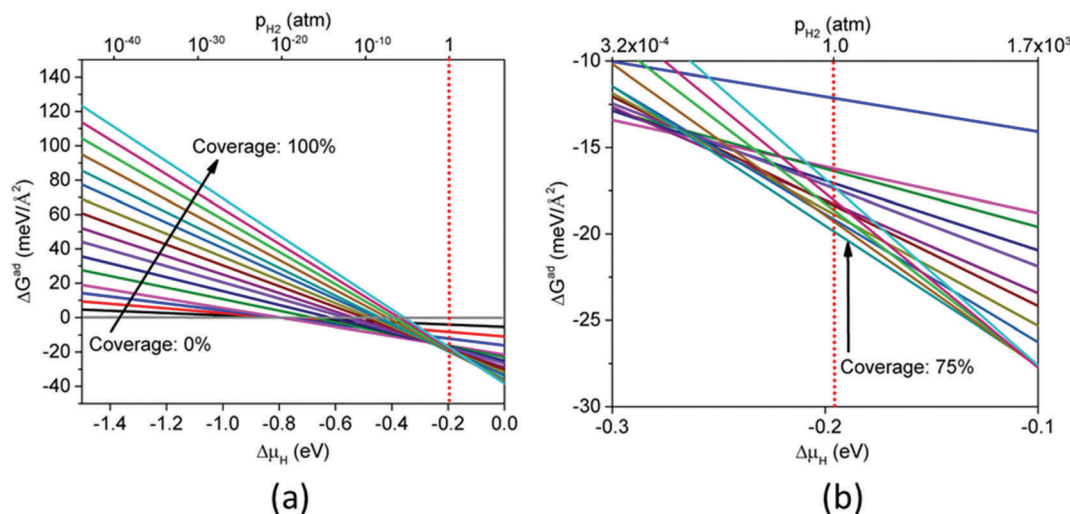

Fig. 6 Gibbs free energy of adsorption (ΔG^{ad}) at 300 K as a function of hydrogen chemical potential ($\Delta \mu_H$) or H$_2$ pressure for CoP(111) with different hydrogen coverages: (a) $\Delta \mu_H$ from −1.5 to 0 eV; (b) $\Delta \mu_H$ from −0.3 to −0.1 eV.

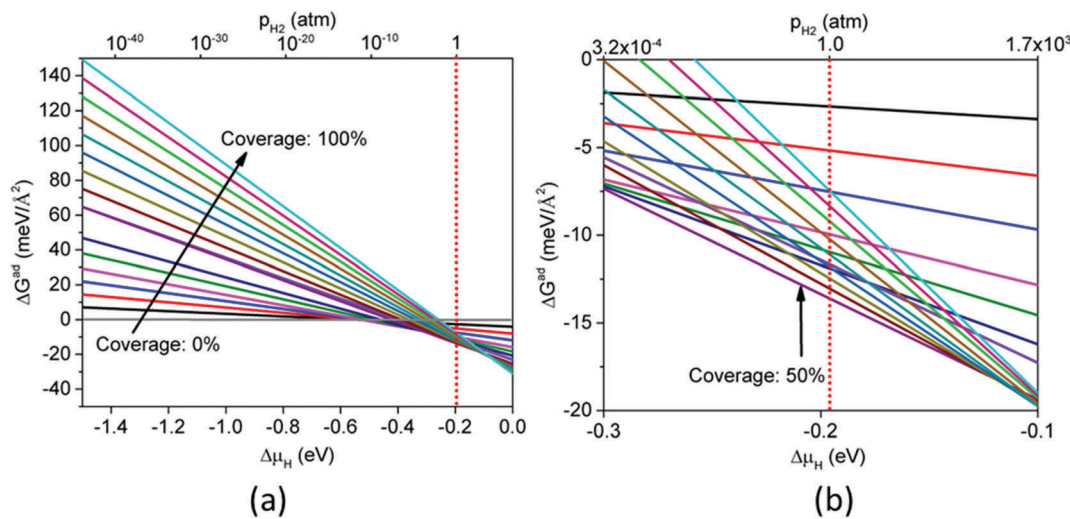**Fig. 8** Gibbs free energy of adsorption (ΔG^{ad}) at 300 K as a function of hydrogen chemical potential ($\Delta\mu_H$) or H_2 pressure for CoP(110) with different hydrogen coverages: (a) $\Delta\mu_H$ from -1.5 to 0 eV; (b) $\Delta\mu_H$ from -0.3 to -0.1 eV.

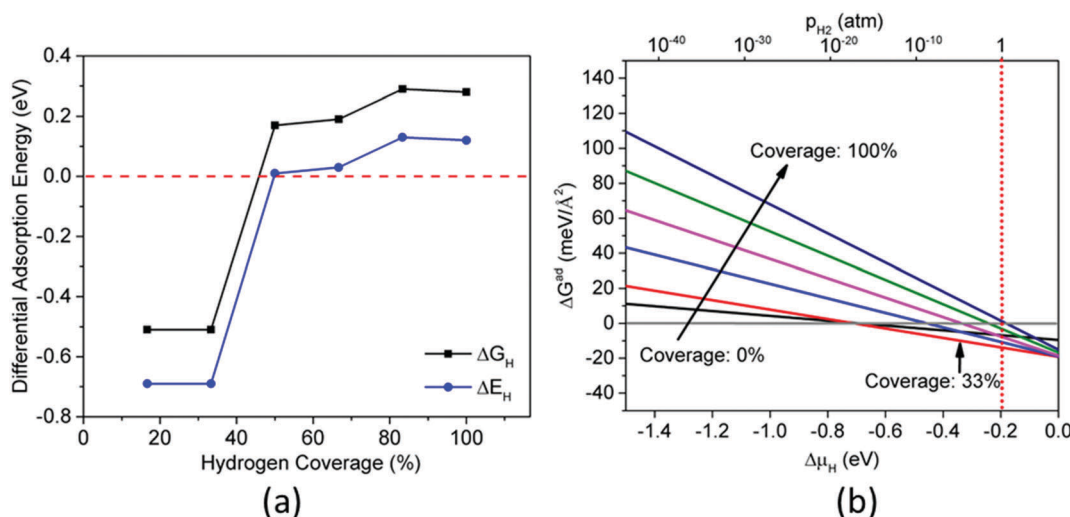**Fig. 9** (a) Differential adsorption energy (ΔE_H) and adsorption free energy (ΔG_H) as a function of hydrogen coverage on CoP(100). (b) Plots of the calculated Gibbs free energy of adsorption (ΔG^{ad}) at 300 K as a function of hydrogen chemical potential ($\Delta\mu_H$) for CoP (100) surface with different hydrogen coverages.

hydrogen atoms occupy cobalt bridge sites. Fig. 10b plots ΔG^{ad} as a function of $\Delta\mu_H$ for CoP(011) at different hydrogen coverages. One can see that 25% hydrogen coverage is the most stable phase at 1 atm and 300 K with $\Delta G^{ad} \sim 0$ meV Å^{-2}, while the clean surface is only slightly higher in energy. This again agrees with the fact that the adsorption of H on CoP(011) is rather weak.

Comparison of (111), (110), (100), and (011) surfaces of CoP

Now that we have studied hydrogen adsorption on the four low Miller-index surfaces of CoP, we can compare them together in terms of stability and HER activity. Using $\Delta G_H \sim 0$ as a criterion, we predict that (111), (110), and (011) surfaces of CoP should have good catalytic activities for HER, while (100) should not. Taking into account *ab initio* atomistic thermo-dynamics, Table 4 shows the comparison of ΔG^{ad} at 1 atm H_2 and 300 K for the most stable coverage of each surface. One can

see that CoP(111) has the most negative ΔG^{ad} followed by (100) and (110), while (011) has a close-to-zero ΔG^{ad}. In other words, at the reaction conditions, the stability trend is (111) > (100) $\sim$ (110) $\gg$ (011). From this perspective, we think that the CoP(111) surface is the most promising facet for high-activity HER.

Our present DFT study of the adsorption of atomic hydrogen on the low-Miller-index surfaces of CoP, including (111), (110), (100), and (011), presents several interesting implications. First, CoP nanostructures that expose different crystal facets would be expected to exhibit different activities for HER catalysis. From our calculated ΔG_H, we predict that (111), (110), and (011) surfaces of CoP will have good catalytic activities for HER. So experimental researchers could prepare highly branched nanostructures that expose a high density of these surfaces. Second, both Co and P on the surfaces play important roles in catalyzing HER. Particularly, on (111) surface, both Co bridge
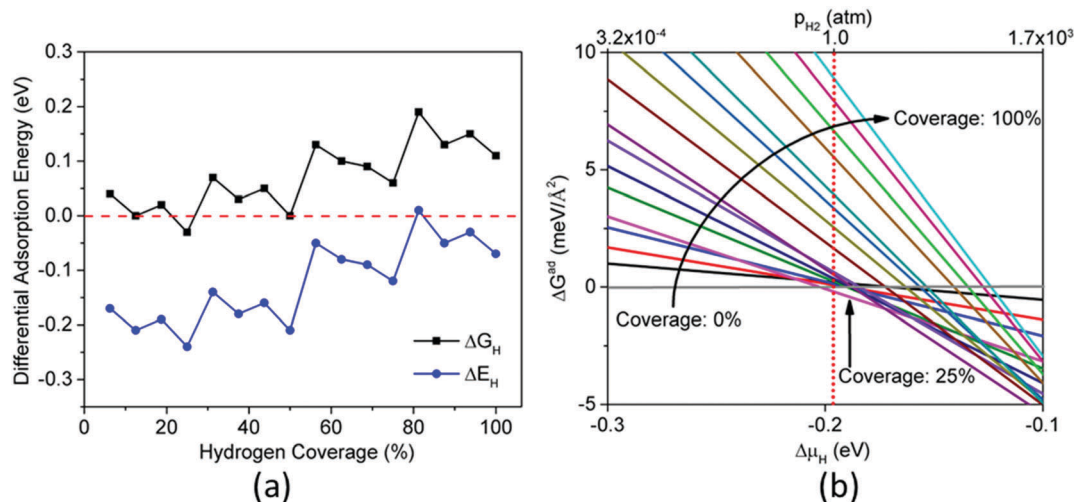
Fig. 10 (a) Differential adsorption energy (ΔE_H) and adsorption free energy (ΔG_H) as a function of hydrogen coverage on CoP(111). (b) Gibbs free energy of adsorption (ΔG^{ad}) at 300 K as a function of hydrogen chemical potential ($\Delta\mu_H$) or H_2 pressure for CoP(011) with different hydrogen coverages.

Table 4 Hydrogen adsorption free energies (ΔG^{ad}) at 1 atm and 300 K of the most stable coverage for each CoP surface

	CoP(111)	CoP(110)	CoP(100)	CoP(011)
ΔG^{ad} (meV Å^{-2})	−19.53	−13.37	−13.56	−0.08

sites and P top sites are found to be able to adsorb hydrogen with a close-to-zero free energy change, indicating that the synergy of proximal Co and P atoms on the surface can result in a better HER activity. Third, hydrogen coverage, pressure, and temperature all have effects on the stabilities of the surfaces. We find that the stabilities of the clean surfaces in vacuum are different from the stabilities at 1 atm H_2 and 300 K. The stabilities of the clean surfaces in vacuum follow the trend of (011) > (110) > (111) > (100), while the stabilities of the surfaces at 1 atm H_2 and 300 K follow the trend of (111) > (100) ∼ (110) ≫ (011). This suggests that if one purposefully prepares the catalyst with the (111) facet, then the catalyst is likely to have a longer lifetime given its high stability during the reaction conditions, while the (011) surface might transform to other more stable surfaces under reaction conditions.

Although the present work focuses on the thermodynamics of HER on different CoP surfaces from computed H adsorption free energy, our results also have interesting implications for the reaction rates. For example, 75% coverage of hydrogen on CoP(111) would be very helpful for the Volmer–Tafel mechanism, as higher surface coverage would increase the chances for two adsorbed hydrogens next to each other to react and form an H_2 molecule. We plan to study the detailed mechanism of HER on CoP surfaces to examine the effect of coverage on reaction kinetics, as recently done for HER on MoS_2.[59]

Conclusions

To shed light on the activity of hydrogen evolution reaction (HER) on CoP, we have studied the adsorption of atomic hydrogen on the low-Miller-index surfaces of CoP, including (111), (110), (100), and (011), by using periodic DFT. From the calculated ΔG_H, we predict that (111), (110), and (011) surfaces will have good catalytic activities for HER. From *ab initio* atomistic thermodynamics, we find that the stabilities of the surfaces at 1 atm H_2 and 300 K follow the trend of (111) > (100) ∼ (110) ≫ (011). So combining ΔG_H and stability, we conclude that the (111) surface of CoP is the most promising facet for high and long-lived HER activity. The key feature of hydrogen adsorption on the (111) is that both Co bridge sites and P top sites are able to adsorb hydrogen with a close-to-zero free energy change and that there is a synergy of proximal Co and P atoms on the CoP(111) surface in adsorbing hydrogen. These insights open a door for further mechanistic understanding of HER on CoP and other phosphides.

Acknowledgements

References

1 W. Lubitz and W. Tumas, *Chem. Rev.*, 2007, **107**, 3900–3903.
2 P. Liu and J. A. Rodriguez, *J. Am. Chem. Soc.*, 2005, **127**, 14871–14878.
3 E. J. Popczun, J. R. McKone, C. G. Read, A. J. Biacchi, A. M. Wiltrout, N. S. Lewis and R. E. Schaak, *J. Am. Chem. Soc.*, 2013, **135**, 9267–9270.
4 L. Feng, H. Vrubel, M. Bensimon and X. Hu, *Phys. Chem. Chem. Phys.*, 2014, **16**, 5917–5921.
5 Z. Huang, Z. Chen, Z. Chen, C. Lv, H. Meng and C. Zhang, *ACS Nano*, 2014, **8**, 8121–8129.

6 A. Laursen, K. Patraju, M. Whitaker, M. Retuerto, T. Sarkar, N. Yao, K. Ramanujachary, M. Greenblatt and G. Dismukes, *Energy Environ. Sci.*, 2015, **8**, 1027–1034.

7 X. Wang, Y. V. Kolen'ko, X. Q. Bao, K. Kovnir and L. Liu, *Angew. Chem., Int. Ed.*, 2015, **54**, 8188–8192.

8 Y. Pan, N. Yang, Y. Chen, Y. Lin, Y. Li, Y. Liu and C. Liu, *J. Power Sources*, 2015, **297**, 45–52.

9 Z. Cai, X. Song, Y. Wang and X. Chen, *ChemElectroChem*, 2015, **2**, 1665–1671.

10 J. Li, J. Li, X. Zhou, Z. Xia, W. Gao, Y. Ma and Y. Qu, *ACS Appl. Mater. Interfaces*, 2016, **8**, 10826–10834.

11 X. Wang, W. Li, D. Xiong, D. Y. Petrovykh and L. Liu, *Adv. Funct. Mater.*, 2016, **26**, 4067–4077.

12 N. Jiang, B. You, M. Sheng and Y. Sun, *ChemCatChem*, 2016, **8**, 106–112.

13 B. You, N. Jiang, M. Sheng, M. W. Bhushan and Y. Sun, *ACS Catal.*, 2016, **6**, 714–721.

14 E. J. Popczun, C. G. Read, C. W. Roske, N. S. Lewis and R. E. Schaak, *Angew. Chem., Int. Ed.*, 2014, **53**, 5427–5430.

15 J. Tian, Q. Liu, A. M. Asiri and X. Sun, *J. Am. Chem. Soc.*, 2014, **136**, 7587–7590.

16 P. Jiang, Q. Liu, C. Ge, W. Cui, Z. Pu, A. M. Asiri and X. Sun, *J. Mater. Chem. A*, 2014, **2**, 14634–14640.

17 Q. Liu, J. Tian, W. Cui, P. Jiang, N. Cheng, A. M. Asiri and X. Sun, *Angew. Chem., Int. Ed.*, 2014, **126**, 6828–6832.

18 Z. Pu, Q. Liu, P. Jiang, A. M. Asiri, A. Y. Obaid and X. Sun, *Chem. Mater.*, 2014, **26**, 4326–4329.

19 F. H. Saadi, A. I. Carim, E. Verlage, J. C. Hemminger, N. S. Lewis and M. P. Soriaga, *J. Phys. Chem. C*, 2014, **118**, 29294–29300.

20 Q. Li, Z. Xing, A. M. Asiri, P. Jiang and X. Sun, *Int. J. Hydrogen Energy*, 2014, **39**, 16806–16811.

21 H. Du, Q. Liu, N. Cheng, A. M. Asiri, X. Sun and C. M. Li, *J. Mater. Chem. A*, 2014, **2**, 14812–14816.

22 Z. Huang, Z. Chen, Z. Chen, C. Lv, M. G. Humphrey and C. Zhang, *Nano Energy*, 2014, **9**, 373–382.

23 E. J. Popczun, C. W. Roske, C. G. Read, J. C. Crompton, J. M. McEnaney, J. F. Callejas, N. S. Lewis and R. E. Schaak, *J. Mater. Chem. A*, 2015, **3**, 5420–5425.

24 J. F. Callejas, C. G. Read, E. J. Popczun, J. M. McEnaney and R. E. Schaak, *Chem. Mater.*, 2015, **27**, 3769–3774.

25 L. Li, X. Li, L. Ai and J. Jiang, *RSC Adv.*, 2015, **5**, 90265–90271.

26 J. A. Vigil and T. N. Lambert, *RSC Adv.*, 2015, **5**, 105814.

27 N. Jiang, B. You, M. Sheng and Y. Sun, *Angew. Chem., Int. Ed.*, 2015, **54**, 6251–6254.

28 B. You, N. Jiang, M. Sheng, S. Gul, J. Yano and Y. Sun, *Chem. Mater.*, 2015, **27**, 7636–7642.

29 M. Liu and J. Li, *ACS Appl. Mater. Interfaces*, 2016, **8**, 2158–2165.

30 Y. Pan, Y. Lin, Y. Chen, Y. Liu and C. Liu, *J. Mater. Chem. A*, 2016, **4**, 4745–4754.

31 H. Huang, C. Yu, J. Yang, C. Zhao, X. Han, Z. Liu and J. Qiu, *ChemElectroChem*, 2016, **3**, 719–725.

32 Y. Tan, H. Wang, P. Liu, C. Cheng, F. Zhu, A. Hirata and M. Chen, *Adv. Mater.*, 2016, **28**, 2951–2955.

33 D.-H. Ha, B. Han, M. Risch, L. Giordano, K. P. C. Yao, P. Karayaylali and Y. Shao-Horn, *Nano Energy*, 2016, DOI: 10.1016/j.nanoen.2016.04.034.

34 J. F. Callejas, J. M. McEnaney, C. G. Read, J. C. Crompton, A. J. Biacchi, E. J. Popczun, T. R. Gordon, N. S. Lewis and R. E. Schaak, *ACS Nano*, 2014, **8**, 11101–11107.

35 P. Jiang, Q. Liu, Y. Liang, J. Tian, A. M. Asiri and X. Sun, *Angew. Chem., Int. Ed.*, 2014, **53**, 12855–12859.

36 Y. Yan, B. Y. Xia, X. Ge, Z. Liu, A. Fisher and X. Wang, *Chemistry*, 2015, **21**, 18062–18067.

37 C. Lv, Z. Peng, Y. Zhao, Z. Huang and C. Zhang, *J. Mater. Chem. A*, 2016, **4**, 1454–1460.

38 C. Y. Son, I. H. Kwak, Y. R. Lim and J. Park, *Chem. Commun.*, 2016, **52**, 2819–2822.

39 J. Tian, Q. Liu, N. Cheng, A. M. Asiri and X. Sun, *Angew. Chem., Int. Ed.*, 2014, **53**, 9577–9581.

40 P. Xiao, M. A. Sk, L. Thia, X. Ge, R. J. Lim, J.-Y. Wang, K. H. Lim and X. Wang, *Energy Environ. Sci.*, 2014, **7**, 2624–2629.

41 J. M. McEnaney, J. C. Crompton, J. F. Callejas, E. J. Popczun, A. J. Biacchi, N. S. Lewis and R. E. Schaak, *Chem. Mater.*, 2014, **26**, 4826–4831.

42 Z. Xing, Q. Liu, A. M. Asiri and X. Sun, *Adv. Mater.*, 2014, **26**, 5702–5707.

43 C. Deng, F. Ding, X. Li, Y. Guo, W. Ni, H. Yan, K. Sun and Y.-M. Yan, *J. Mater. Chem. A*, 2016, **4**, 59–66.

44 Z. Yao, Y. Su, C. Lu, C. Yang, Z. Xu, J. Zhu, X. Zhuang and F. Zhang, *New J. Chem.*, 2016, **40**, 6015–6021.

45 Z. Pu, S. Wei, Z. Chen and S. Mu, *Appl. Catal., B*, 2016, **196**, 193–198.

46 J. M. McEnaney, J. C. Crompton, J. F. Callejas, E. J. Popczun, C. G. Read, N. S. Lewis and R. E. Schaak, *Chem. Commun.*, 2014, **50**, 11026–11028.

47 T. Erdey-Gruz and M. Volmer, *Z. Phys. Chem. A*, 1930, **150**, 203.

48 J. Heyrovský, *Recl. Trav. Chim. Pays-Bas*, 1927, **46**, 582–585.

49 J. Tafel, *Z. Phys. Chem.*, 1905, **50**, 641.

50 J. K. Nørskov, T. Bligaard, A. Logadottir, J. R. Kitchin, J. G. Chen, S. Pandelov and U. Stimming, *J. Electrochem. Soc.*, 2005, **152**, J23–J26.

51 G. Kresse and J. Furthmüller, *Phys. Rev. B: Condens. Matter Mater. Phys.*, 1996, **54**, 11169–11186.

52 P. E. Blöchl, *Phys. Rev. B: Condens. Matter Mater. Phys.*, 1994, **50**, 17953–17979.

53 J. P. Perdew, K. Burke and M. Ernzerhof, *Phys. Rev. Lett.*, 1996, **77**, 3865–3868.

54 W. Tang, E. Sanville and G. Henkelman, *J. Phys.: Condens. Matter*, 2009, **21**, 084204.

55 C. Campaná, B. Mussard and T. K. Woo, *J. Chem. Theory Comput.*, 2009, **5**, 2866–2878.

56 J. Rogal and K. Reuter, *Experiment, Modeling and Simulation of Gas Surface Interactions for Reactive Flows in Hypersonic Flights*, 2007, pp. 2-1–2-18.

57 D. R. Stull and H. Prophet, *JANAF thermochemical tables*, DTIC Document, 1971.

58 S. Rundqvist, *Acta Chem. Scand.*, 1962, **16**, 287–292.

59 Q. Tang and D. E. Jiang, *ACS Catal.*, 2016, **6**, 4953–4961.